Analysis of resonant inelastic x-ray scattering from Sr$_2$IrO$_4$ in an itinerant-electron approach

Jun-ichi Igarashi[1] and Tatsuya Nagao[2]

[1]*Faculty of Science, Ibaraki University, Mito, Ibaraki 310-8512, Japan*
[2]*Faculty of Engineering, Gunma University, Kiryu, Gunma 376-8515, Japan*

We analyze the resonant x-ray scattering (RIXS) spectra from Sr$_2$IrO$_4$ in an itinerant-electron approach. Employing a multiorbital tight-binding model on the square lattice, we calculate the one-electron energy band within the Hartree-Fock approximation, which leads to an antiferromagnetic ground state. We then evaluate the two-particle Green's functions for the particle-hole pair excitations within the random phase approximation, which are connected to the RIXS spectra within the fast collision approximation. The calculated RIXS spectra exhibit a two-peak structure with slightly different energies in the low-energy region, which originate from the bound states in the two-particle Green's function. They may be interpreted as the split modes of a magnon. We also obtain several δ-function peaks, which arise from the bound states around the bottom of the energy continuum. They may be called exciton modes. These characteristics are in qualitative agreement with the RIXS experiment, demonstrating that the weak coupling theory could explain both the magnon and the exciton peaks in the RIXS spectra on an equal footing.

I. INTRODUCTION

Strong synchrotron sources have been rapidly developing, and resonant inelastic x-ray scattering (RIXS) has become a powerful tool to probe elementary excitations in solids [1,2]. Both the K- and L-edge resonances are utilized in transition-metal compounds. On the K-edge resonance, the $1s$ core electron is prompted to empty p-symmetric states by absorbing photons, then the photoexcited electron is recombined with the core hole by emitting photons. In this process, charge excitations are created to screen the core-hole potential in the intermediate state. Note that two magnons could also be created in magnetic systems [3–6], since the exchange coupling is modified around the core-hole site in the presence of the core-hole potential.

On the L-edge resonance, on the other hand, the $2p$ core electron is prompted to empty d-symmetric states by absorbing photons, then an electron that is occupied on the d-symmetric state is combined with the core hole by emitting photons. Since the electron combined with the core hole is not necessarily the same as the photoexcited electron, the particle-hole pair excitations could be directly created in the d-symmetric states in addition to the screening effect of the core-hole potential in the intermediate state. Note that the $2p$ core states are split into two well-separated levels with the total angular momentum $j_c = 1/2$ and $j_c = 3/2$ due to the strong spin-orbit interaction (SOI). The corresponding L edges are discriminated as the L_2 and L_3 edges, respectively. Owing to this split, single spin-flip excitations could be created. Actually, the spectral peaks as a function of energy loss are found to follow the dispersion of spin waves in the Heisenberg model with changing momentum transfer in undoped cuprates [7–9]. Such L-edge RIXS spectra have been analyzed on the spin model within the fast collision approximation (FCA), which is justified when the core-hole lifetime broadening width is larger than the concerned excitation energy [10–12]. Although only the one-magnon excitations could be created within the FCA, the experimental energy profile shows an asymmetric shape [7–9], indicating that two-magnon excitations are involved in

addition to one-magnon excitations. An analysis going beyond the FCA has been carried out to explain the asymmetrical profile, in quantitative agreement with the experiment [13–15].

Recently, RIXS experiments have been carried out at the Ir L_3 edge in Sr$_2$IrO$_4$ [16,17]. This material shows antiferromagnetism at low temperatures below $\sim$230 K [18–20]. Its ordering is concerned with the spin-orbit coupled *isospin* $j_{\text{eff}} = 1/2$, since the SOI is large on the $5d$ states of Ir [21]. The low-energy peak behaves as a one-magnon peak in undoped cuprates [17], while other peaks emerge around $\omega \sim 0.5$ eV with substantial weights as a function of energy loss ω. The RIXS spectra have been analyzed within the FCA on the basis of the localized electron model [22,23]. Note that the FCA is expected to work well for this material, since the $2p$ core hole has a lifetime broadening width as large as 2.5–3.5 eV [24], which is much larger than the concerned excitation energies. The low-energy peak has been interpreted as the magnetic excitation (magnon) in the isospin space $j_{\text{eff}} = 1/2$, while the peak around $\omega \sim 0.5$ eV as the excitation (exciton) from the $j_{\text{eff}} = 3/2$ manifold to the $j_{\text{eff}} = 1/2$ manifold [25]. Recently, the magnon mode has been predicted to be split into two modes due to the interplay between Hund's coupling and the SOI, and a detailed analysis of the magnon peak has been made by taking account of the mode splitting [23,26].

Although the localized electron model has been successful in analyzing the RIXS spectra, there remain issues that the itinerancy of the electrons might play a key role to elucidate the physical features of Sr$_2$IrO$_4$. For instance, it has been argued as to whether the system behaves as a Mott insulator or a band insulator [27,28]. It is also established that the isotropic Heisenberg model can reproduce magnon dispersion only when it includes second- and third-nearest-neighbor exchange coupling in addition to first-nearest-neighbor exchange coupling [29]. Such observations have naturally prompted us to investigate the material in the itinerant-electron approach, and several attempts have been carried out to study its electronic structure. The band structure calculation has been carried out within the local density approximation augmented by the Coulomb interaction (LDA+U), leading to antiferromagnetic

ordering and the associated energy gap in the one-electron energy band [30]. The electron correlation effects have been taken into account by the variational method [31] as well as by the dynamical mean field theory [27]. Recently, excitation spectra have been investigated by calculating the spectral function of the two-particle Green's function for particle-hole pair excitations within the Hartree-Fock approximation (HFA) and the random phase approximation (RPA) [32], showing that they are composed of magnons and excitons. However, a direct comparison between the spectral function and the RIXS spectrum cannot be allowed, since the former is different from the RIXS spectra due to the second-order optical process.

The purpose of this paper is to analyze the RIXS spectra with an argument based on an itinerant-electron picture. Introducing the multiorbital tight-binding model, we calculate the one-electron energy band within the HFA, where the antiferromagnetic ground state is realized. Then, on this ground state, we calculate the two-particle Green's function for the particle-hole pair excitations within the RPA. Magnons appear as bound states below the energy continuum, and are split into two modes. Several other bound states emerge around the bottom of the energy continuum [33]. These, together with the continuum states (often containing resonant modes), may constitute exciton modes.

The spectral functions of the two-particle Green's function are related to the RIXS spectra within the FCA, which is known to work well for the RIXS spectra in Sr_2IrO_4. For magnons split into two modes, the two-peak structures are found with a significant momentum dependence of intensities. The splitting of the magnon modes, however, has not been confirmed yet by RIXS experiments, probably because the experimental energy resolution is as large as 40 meV. Furthermore, sharp exciton peaks emerge with their intensities larger than the magnon intensities, being separated from the magnon peaks, in consistence with the RIXS experiment. Thus it is demonstrated that the weak coupling approach of the HFA and RPA could explain both the magnon and the exciton peaks in the RIXS spectra on an equal footing, providing a good starting point of taking account of electron correlations.

The present paper is organized as follows. In Sec. II, we introduce a multiorbital tight-binding model, and study the electronic structure within the HFA. In Sec. III, we describe the dipole process, and calculate the absorption coefficient at the L edge. In Sec. IV, we derive the formula for the RIXS spectra within the FCA. In Sec. V, comparisons are made between the calculated and experimental RIXS spectra. Section VI is devoted to the concluding remarks.

II. ELECTRONIC STRUCTURE

A. Model Hamiltonian

Transition-metal oxide Sr_2IrO_4 with a K_2NiF_4-type structure is composed of an IrO_2 layer separated by a Sr-O layer [18]. Since the crystal field energy of the e_g orbitals is about 2 eV higher than that of the t_{2g} orbitals, we consider only t_{2g} orbitals with five electrons occupying each Ir atom. Since the oxygen octahedra surrounding an Ir atom are rotated about the crystallographic c axis by about 11° [31,34], the t_{2g} states are defined in the local coordinate frames rotated in accordance

with the rotation of octahedra. For simplicity, we disregard the fact that the degenerate t_{2g} levels are split by the tetragonal crystal field due to the rotation and distortion of IrO_6 octahedra. Then, we start from the multiorbital Hubbard model on the square lattice in the local coordinate frames,

$$H = H_{kin} + H_{SO} + H_I, \tag{2.1}$$

where H_{kin}, H_{SO}, and H_I are described by the annihilation ($d_{in\sigma}$) and creation ($d_{in\sigma}^\dagger$) operators of an electron with orbital n ($= yz, zx, xy$) and spin σ at the Ir site i as follows:

$$H_{kin} = \sum_{\langle i,i'\rangle} \sum_{n,n',\sigma} t_{in,i'n'} d_{in\sigma}^\dagger d_{i'n'\sigma} + \text{H.c.}, \tag{2.2}$$

$$H_{SO} = \zeta_{SO} \sum_i \sum_{n,n',\sigma,\sigma'} d_{in\sigma}^\dagger (\mathbf{L})_{nn'} \cdot (\mathbf{S})_{\sigma\sigma'} d_{in'\sigma'}, \tag{2.3}$$

$$\begin{aligned} H_I = &U \sum_{i,n} n_{in\uparrow} n_{in\downarrow} \\ &+ \sum_{i,n<n',\sigma} [U' n_{in\sigma} n_{in'-\sigma} + (U' - J) n_{in\sigma} n_{in'\sigma}] \\ &+ J \sum_{i,n\neq n'} (d_{in\uparrow}^\dagger d_{in'\downarrow}^\dagger d_{in\downarrow} d_{in'\uparrow} + d_{in\uparrow}^\dagger d_{in\downarrow}^\dagger d_{in'\downarrow} d_{in'\uparrow}). \end{aligned}$$
$$\tag{2.4}$$

The intersite interaction H_{kin} stands for the kinetic energy. The transfer integral $t_{in,i'n'}$ exhibits a highly anisotropic nature. An electron on the xy orbital could transfer to the xy orbital in the nearest-neighbor sites through the intervening O $2p$ orbitals, while an electron on the $yz(zx)$ orbital could transfer to the $yz(zx)$ orbital in the nearest-neighbor sites only along the $y(x)$ direction. The nonzero values of $t_{in,i'n'}$'s are assumed to be the same and are denoted as t_1. The SOI of 5d electrons is denoted as H_{SO}, with $\mathbf{L}$ and $\mathbf{S}$ denoting the orbital and spin angular momentum operators. The H_I represents the Coulomb interaction between electrons with $\nu = (n,\sigma)$. Parameters satisfy $U = U' + 2J$ [35]. We use the values $U = 1.4$ eV and $J/U = 0.15$ in the following calculation. As regards the transfer integral t_1 and the SOI parameter ζ_{SO}, we consider two typical parameter sets; one is that $\zeta_{SO} = 0.36$ eV, $t_1 = 0.36$ eV (case A), and another is that $\zeta_{SO} = 0.45$ eV, $t_1 = 0.25$ eV (case B). The values in case A are the same as in Ref. [36], and give the one-electron bandwidth that is consistent with the band calculation based on the local density approximation [30,32]. The smaller value of t_1 in case B may lead to a larger energy gap in the one-electron band. Note that the smaller values of t_1 around 0.1–0.2 eV have been estimated on the basis of a localized picture [37].

B. Hartree-Fock approximation

A unit cell j contains two atoms at $\mathbf{r}_j$ and at $\mathbf{r}_j + \mathbf{a}$, where $\mathbf{a} = (a,0)$, with a a nearest-neighbor distance. We introduce the Fourier transform of the annihilation operator with the wave vector $\mathbf{k}$ in the magnetic Brillouin zone (MBZ), which is defined as the half of the first Brillouin zone:

$$d_{\lambda n\sigma}(\mathbf{k}) = \sqrt{\frac{2}{N}} \sum_j d_{j'n\sigma} e^{-i\mathbf{k}\cdot\mathbf{r}_j}, \tag{2.5}$$

where j runs over unit cells and $N/2$ stands for the number of the unit cells. We assign $\lambda = 1$ and 2 for the A and B sublattices, respectively. The index j' specifies the site within the jth unit cell as $\mathbf{r}_{j'} = \mathbf{r}_j$ and $\mathbf{r}_j + \mathbf{a}$ for $\lambda = 1$ and 2, respectively. Then, the one-electron energy $H_0 \equiv H_{\mathrm{kin}} + H_{\mathrm{SO}}$ may be rewritten as

$$H_0 = \sum_{\mathbf{k}\xi\xi'} d_\xi^\dagger(\mathbf{k})[\hat{H}_0(\mathbf{k})]_{\xi,\xi'} d_{\xi'}(\mathbf{k}), \quad (2.6)$$

with abbreviations $\xi = (\lambda, n, \sigma)$ and $\xi' = (\lambda', n', \sigma')$.

Arranging ξ in order $(1, yz, \uparrow)$, $(1, zx, \uparrow)$, $(1, xy, \uparrow)$, $(1, yz, \downarrow)$, $(1, zx, \downarrow)$, $(1, xy, \downarrow)$, $(2, yz, \uparrow)$, $(2, zx, \uparrow)$, $(2, xy, \uparrow)$, $(2, yz, \downarrow)$, $(2, zx, \downarrow)$, $(2, xy, \downarrow)$, we have $\hat{H}_0(\mathbf{k})$ in a block form,

$$\hat{H}_0(\mathbf{k}) = \begin{pmatrix} \hat{H}_{AA}^0(\mathbf{k}) & \hat{H}_{AB}^0(\mathbf{k}) \\ \hat{H}_{BA}^0(\mathbf{k}) & \hat{H}_{BB}^0(\mathbf{k}) \end{pmatrix}, \quad (2.7)$$

where

$$\hat{H}_{AA}^0(\mathbf{k}) = \hat{H}_{BB}^0(\mathbf{k}) = \frac{\zeta_{\mathrm{SO}}}{2} \begin{pmatrix} 0 & i & 0 & 0 & 0 & -1 \\ -i & 0 & 0 & 0 & 0 & i \\ 0 & 0 & 0 & 1 & -i & 0 \\ 0 & 0 & 1 & 0 & -i & 0 \\ 0 & 0 & i & i & 0 & 0 \\ -1 & -i & 0 & 0 & 0 & 0 \end{pmatrix}, \quad (2.8)$$

$$\hat{H}_{AB}^0(\mathbf{k}) = [\hat{H}_{BA}^0(\mathbf{k})]^\star$$
$$= \begin{pmatrix} t_1(\mathbf{k}) & 0 & 0 & 0 & 0 & 0 \\ 0 & t_2(\mathbf{k}) & 0 & 0 & 0 & 0 \\ 0 & 0 & t_3(\mathbf{k}) & 0 & 0 & 0 \\ 0 & 0 & 0 & t_1(\mathbf{k}) & 0 & 0 \\ 0 & 0 & 0 & 0 & t_2(\mathbf{k}) & 0 \\ 0 & 0 & 0 & 0 & 0 & t_3(\mathbf{k}) \end{pmatrix}. \quad (2.9)$$

Here the dispersion may be expressed as

$$t_n(\mathbf{k}) = -2t_1 e^{-ik_x} \times \begin{cases} \cos k_y, & \text{for} \quad n = 1, \\ \cos k_x, & \text{for} \quad n = 2, \\ (\cos k_x + \cos k_y), & \text{for} \quad n = 3, \end{cases} \quad (2.10)$$

where $\mathbf{k}$ is measured in units of $1/a$.

We follow the conventional procedure of the HFA as explained in Ref. [38]. Rewriting $H_I = \frac{1}{2} \sum_i \sum_{\nu_1, \nu_2, \nu_3, \nu_4} g(\nu_1 \nu_2; \nu_3 \nu_4) d_{i\nu_1}^\dagger d_{i\nu_2}^\dagger d_{i\nu_4} d_{i\nu_3}$, we replace H_I with

$$H_I^{\mathrm{HF}} = \frac{1}{2} \sum_j \sum_{\xi_1, \xi_2, \xi_3, \xi_4} \Gamma^{(0)}(\xi_1 \xi_2; \xi_3 \xi_4) \langle d_{j\xi_2}^\dagger d_{j\xi_4} \rangle d_{j\xi_1} d_{j\xi_3}, \quad (2.11)$$

where $\Gamma^{(0)}$ is the antisymmetric vertex function,

$$\Gamma^{(0)}(\xi_1 \xi_2; \xi_3 \xi_4) = g(\xi_1 \xi_2; \xi_3 \xi_4) - g(\xi_1 \xi_2; \xi_4 \xi_3), \quad (2.12)$$

with $\xi = (\lambda, \nu)$. Here, $d_{j\xi} = d_{j(\lambda\nu)}$ denotes the annihilation operator of the d electron with the ν spin-orbital state at the site belonging to the sublattice λ in the jth unit cell. Then, we

introduce the single-particle Green's function in a matrix form with 12×12 dimensions,

$$[\hat{G}(\mathbf{k},\omega)]_{\xi,\xi'} = -i \int \langle T[d_\xi(\mathbf{k},t) d_{\xi'}^\dagger(\mathbf{k},0)] \rangle e^{i\omega t} dt, \quad (2.13)$$

where T is the time ordering operator, and $\langle X \rangle$ denotes the ground-state average of operator X. The Green's function is obtained by solving the equations of motion, resulting in

$$[\hat{G}(\mathbf{k},\omega)]_{\xi,\xi'} = \sum_\ell \frac{[\hat{U}(\mathbf{k})]_{\xi,\ell} [\hat{U}(\mathbf{k})^{-1}]_{\ell,\xi'}}{\omega - E_\ell(\mathbf{k}) + i\epsilon \, \mathrm{sgn}[E_\ell(\mathbf{k})]}, \quad (2.14)$$

where $\mathrm{sgn}[A]$ stands for a sign of quantity A and δ denotes a positive convergent factor. The ℓth energy eigenvalue within the HFA is written as $E_\ell(\mathbf{k})$ measured from the chemical potential. The definition of the unitary matrix $\hat{U}(\mathbf{k})$ is found in Ref. [38]. The Green's function contains the expectation values of the electron density operator on the ground state, which are self-consistently determined from

$$\langle a_\xi^\dagger a_{\xi'} \rangle = \frac{2}{N} \sum_\mathbf{k} \int [-i\hat{G}(\mathbf{k},\omega)]_{\xi,\xi'} e^{i\omega 0^+} \frac{d\omega}{2\pi}. \quad (2.15)$$

This equation is solved by iteration with summing over $\mathbf{k}$ by dividing the MBZ into 100×100 meshes. We obtain a self-consistent solution of the antiferromagnetic order with the staggered magnetic moment along the x axis as the ground state, which is consistent with the magnetic measurements [18,19]. Both the orbital and the spin moments are induced due to the strong SOI; $\langle S_x \rangle = \pm 0.112$ (case A) and ± 0.143 (case B), while $\langle L_x \rangle = \pm 0.435$ (case A) and ± 0.551 (case B). The antiferromagnetic order in the local coordinate frames indicates that a weak ferromagnetic moment is induced in the coordinate frame fixed to the crystal axes. The one-electron energy has a finite gap due to the antiferromagnetic order.

III. DIPOLE TRANSITION AND ABSORPTION SPECTRA

A. Dipole transition

For the interaction between the photon and matter, we consider the dipole transition at the L edge, where the $2p$ core electron is excited to the $5d$ states by absorbing photons (and the reverse process). This process may be described by the interaction

$$H_x = \sum_{\lambda, n, \sigma, j_c, m, \alpha} w(n\sigma; j_c m; \alpha)$$
$$\times \sum_{\mathbf{k},\mathbf{q}} d_{\lambda n\sigma}^\dagger(\mathbf{k}+\mathbf{q}) p_{\lambda j_c m}(\mathbf{k}) c_\alpha(\mathbf{q}) v(\lambda, \mathbf{q}) + \mathrm{H.c.}, \quad (3.1)$$

where $c_\alpha(\mathbf{q})$ is the annihilation operator of a photon with momentum $\mathbf{q}$ and polarization α. The $p_{\lambda j_c m}(\mathbf{k})$ is the annihilation operator of a core electron belonging to the λ site with wave vector $\mathbf{k}$ and the angular momentum $j_c = 3/2$ and $1/2$ and magnetic quantum number m. The $v(\lambda, \mathbf{q})$ stands for the extra phase on the B sites, which is explicitly defined as

$$v(\lambda, \mathbf{q}) = \delta_{\lambda,1} + \delta_{\lambda,2} e^{iq_x}. \quad (3.2)$$

Note that, when $\mathbf{k} + \mathbf{q}$ lies outside the first MBZ, it is reduced back to the inside of the first MBZ by a reciprocal lattice vector in the reduced zone scheme. The $w(n\sigma; j_c m; \alpha)$ represents

TABLE I. $w(n\sigma; j_c m; \alpha)$ within the t_{2g} basis with $j_c = \frac{3}{2}$ and $\frac{1}{2}$.

α	$(n\sigma) \setminus m$	$\frac{3}{2}$	$\frac{1}{2}$	$-\frac{1}{2}$	$-\frac{3}{2}$	$\frac{1}{2}$	$-\frac{1}{2}$
		$j_c = \frac{3}{2}$				$j_c = \frac{1}{2}$	
x	$(zx \uparrow)$	0	$\frac{\sqrt{2}}{\sqrt{15}}$	0	0	$\frac{1}{\sqrt{15}}$	0
	$(zx \downarrow)$	0	0	$\frac{\sqrt{2}}{\sqrt{15}}$	0	0	$-\frac{1}{\sqrt{15}}$
	$(xy \uparrow)$	$-\frac{i}{\sqrt{10}}$	0	$-\frac{i}{\sqrt{30}}$	0	0	$-\frac{i}{\sqrt{15}}$
	$(xy \downarrow)$	0	$-\frac{i}{\sqrt{30}}$	0	$-\frac{i}{\sqrt{10}}$	$\frac{i}{\sqrt{15}}$	0
y	$(yz \uparrow)$	0	$\frac{\sqrt{2}}{\sqrt{15}}$	0	0	$\frac{1}{\sqrt{15}}$	0
	$(yz \downarrow)$	0	0	$\frac{\sqrt{2}}{\sqrt{15}}$	0	0	$-\frac{1}{\sqrt{15}}$
	$(xy \uparrow)$	$-\frac{1}{\sqrt{10}}$	0	$\frac{1}{\sqrt{30}}$	0	0	$\frac{1}{\sqrt{15}}$
	$(xy \downarrow)$	0	$-\frac{1}{\sqrt{30}}$	0	$\frac{1}{\sqrt{10}}$	$\frac{1}{\sqrt{15}}$	0
z	$(yz \uparrow)$	$-\frac{i}{\sqrt{10}}$	0	$-\frac{i}{\sqrt{30}}$	0	0	$-\frac{i}{\sqrt{15}}$
	$(yz \downarrow)$	0	$-\frac{i}{\sqrt{30}}$	0	$-\frac{i}{\sqrt{10}}$	$\frac{i}{\sqrt{15}}$	0
	$(zx \uparrow)$	$-\frac{1}{\sqrt{10}}$	0	$\frac{1}{\sqrt{30}}$	0	0	$\frac{1}{\sqrt{15}}$
	$(zx \downarrow)$	0	$-\frac{1}{\sqrt{30}}$	0	$\frac{1}{\sqrt{10}}$	$\frac{1}{\sqrt{15}}$	0

the matrix elements of the $2p \to 5d$ transition. Table I lists the values for $\alpha = x, y, z$ corresponding to the polarization directing to the x, y, z axes.

B. Absorption coefficient at the L edge

X rays could be absorbed by exciting the $2p$ electron to unoccupied levels at the L edge. Since the core states are well localized in real space, the absorption coefficient is given by summing the intensity at each site. Neglecting the interaction between the excited electron and the core hole left behind, we have the expression of the absorption coefficient as

$$
A(\omega_i, j_c) \propto \frac{2}{N} \sum_{\alpha, m} \sum_{\mathbf{k}, \ell} \sum_{\xi, \xi'} w(n\sigma; j_c m; \alpha) w^*(n'\sigma'; j_c m; \alpha)
$$

$$
\times \delta_{\lambda, \lambda'} U_{\xi, \ell}^*(\mathbf{k}) U_{\xi', \ell}(\mathbf{k}) \frac{1 - n_\ell(\mathbf{k})}{[\omega_i - E_\ell(\mathbf{k}) + \epsilon_{2p}(j_c)]^2 + \Gamma_c^2},
$$
$$(3.3)$$

where $\xi = (\lambda, n, \sigma)$ and $\xi' = (\lambda', n', \sigma')$. The occupation number of the eigenstate with energy $E_\ell(\mathbf{k})$ is given by $n_\ell(\mathbf{k})$. The ω_i and $\epsilon_{2p}(j_c)$ represent the energies of the incident photon and of the $2p$ core-hole level in the j_c manifold, respectively. The lifetime broadening width of the core hole is given by Γ_c. Note that polarizations are averaged over in Eq. (3.3).

Figure 1 shows the calculated absorption coefficient with $\Gamma_c = 2.5$ eV for the parameters in case A. The origin of energy is set to be the difference between the bottom of the conduction band and each core-level energy. Since the conduction bandwidth is of order 1 eV, which is smaller than Γ_c, the spectral shape looks quite similar to the Lorentzian shape. Note that the interaction between the $2p$ core hole and the excited electron would make the spectral shape sharper. The intensity at the L_2 edge is found to be much smaller than that at the L_3 edge, in agreement with the experiment and the analysis with the localized states in the $j_{\text{eff}} = \frac{1}{2}$ manifold [39,40]. The present result accordingly indicates that
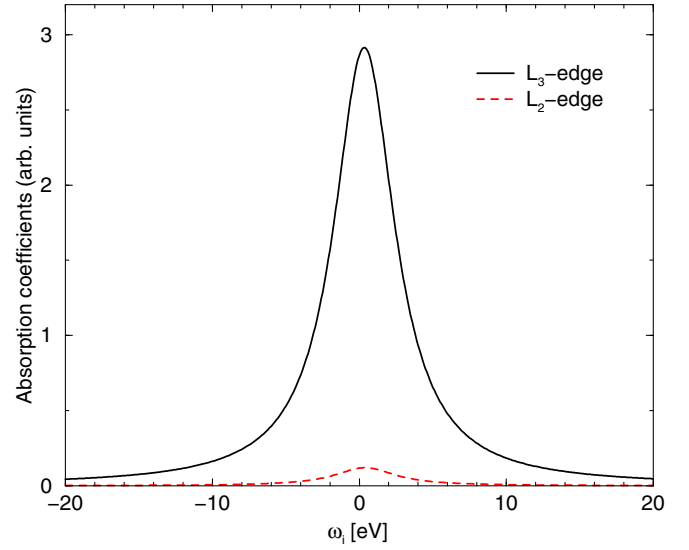

FIG. 1. (Color online) Absorption coefficients $A(\omega_i, j_c)$ as a function of x-ray energy with $\Gamma_c = 2.5$ eV in case A. The (black) solid and the (red) dashed lines are spectra at the Ir L_3 and L_2 edges, respectively. The origin of the energy is set to be the difference between the bottom of the conduction band and the core-level energy. The absorption coefficients for the parameters in case B are almost the same as in case A.

the conduction band given by the HFA is mainly composed of the states in the $j_{\text{eff}} = \frac{1}{2}$ manifold. The absorption coefficients for the parameters in case B are almost the same as in case A.

IV. FORMULA FOR RIXS SPECTRA

A. Second-order optical process

The RIXS spectral intensity may be expressed as the second-order optical process,

$$
W(\omega_i, q; \alpha_i, \alpha_f) = 2\pi \sum_f \left| \sum_n \frac{\langle \Phi_f | H_x | \Phi_n \rangle \langle \Phi_n | H_x | \Phi_i \rangle}{\omega_i + \epsilon_g - \epsilon_n + i\Gamma_c} \right|^2
$$

$$
\times \delta(\omega_i + \epsilon_g - \omega_f - \epsilon_f). \tag{4.1}
$$

The initial state is given by $|\Phi_i\rangle = c_{\alpha_i}^\dagger(\mathbf{q}_i)|0\rangle|g\rangle$, where $|g\rangle$ represents the ground state of the matter with energy ϵ_g, and $|0\rangle$ denotes the vacuum state with photons. The intermediate state is given by $|\Phi_n\rangle = |0\rangle|n\rangle$, where $|n\rangle$ stands for the intermediate state of the matter with energy ϵ_n. The final state is given by $|\Phi_f\rangle = c_{\alpha_f}^\dagger(\mathbf{q}_f)|0\rangle|f\rangle$, where $|f\rangle$ represents the final state of the matter with energy ϵ_f. The incident photon has momentum and energy $q_i = (\mathbf{q}_i, \omega_i)$, and polarization α_i, while the scattered photon has momentum and energy $q_f = (\mathbf{q}_f, \omega_f)$, and polarization α_f. The momentum and energy transferred to the matter are accordingly given by $q = q_i - q_f = (\mathbf{q}, \omega)$.

In this second-order process, the dipole transition creates the $(5d)^6$ configuration at the core-hole site in the intermediate state. This state would be relaxed by hopping the excited electron to neighboring sites. Since the conduction band has a width of at most 1 eV while Γ_c is as large as 2.5 eV, the energy denominator of Eq. (4.1) could be factored out with reasonable accuracy. It may be hard to additionally create electron-hole pairs in the intermediate state, since the $(5d)^6$ configuration is

almost kept at the core-hole site. Therefore, Eq. (4.1) may be approximated as

$$W(\omega_i, q; \alpha_i, \alpha_f) = 2\pi |R(\omega_i, E_0)|^2$$

$$\times \sum_f \left| \sum_n \langle \Phi_f | H_x | \Phi_n \rangle \langle \Phi_n | H_x | \Phi_i \rangle \right|^2$$

$$\times \delta(\omega + \epsilon_g - \epsilon_f), \qquad (4.2)$$

where

$$R(\omega_i, E_0) = \frac{1}{\omega_i - E_0 + \epsilon_{2p}(j_c) + i\Gamma_c}. \qquad (4.3)$$

Equation (4.3) arises from the energy denominator factored out with E_0 being a typical energy of the conduction band. Moreover, the intensity is rewritten as

$$W(\omega_i, q; \alpha_i, \alpha_f) = |R(\omega_i, E_0)|^2 \hat{M}^\dagger(\mathbf{q}, \alpha_i, \alpha_f; j_c) \hat{Y}^{+-}(q)$$

$$\times \hat{M}(\mathbf{q}, \alpha_i, \alpha_f; j_c), \qquad (4.4)$$

where

$$[\hat{Y}^{+-}(\mathbf{q}, \omega)]_{\xi_1 \xi_1'; \xi \xi'} = \int_{-\infty}^{\infty} \langle [\rho_{\mathbf{q}\xi_1\xi_1'}(t)]^\dagger \rho_{\mathbf{q}\xi\xi'}(0) \rangle e^{i\omega t} dt, \quad (4.5)$$

with

$$\rho_{\mathbf{q}\xi\xi'} = \sqrt{\frac{2}{N}} \sum_{\mathbf{k}} d_\xi^\dagger(\mathbf{k} + \mathbf{q}) d_{\xi'}(\mathbf{k}). \qquad (4.6)$$

Here $\mathbf{k} + \mathbf{q}$ is to be reduced back to the MBZ by a reciprocal vector $\mathbf{G}$, when it lies outside the MBZ. The $\hat{Y}^{+-}(q)$ represents the correlation function of the electron-hole pair excitations, which is a matrix of 144×144 dimensions. The $\hat{M}(\mathbf{q}, \alpha_i, \alpha_f; j_c)$ is regarded as a vector with 144 dimensions, defined by

$$[\hat{M}(\mathbf{q}, \alpha_i, \alpha_f; j_c)]_{\xi\xi'} = \delta_{\lambda, \lambda'} v(\lambda, \mathbf{q})$$

$$\times \sum_m \sum_{\alpha, \beta = x, y, z} (\alpha_i)_\alpha w(n\sigma; j_c m; \alpha)$$

$$\times w^*(n'\sigma'; j_c m; \beta)(\alpha_f)_\beta, \qquad (4.7)$$

with $\xi = (\lambda, n, \sigma)$ and $\xi' = (\lambda', n', \sigma')$. Since the scattering event takes place within a single site, we have the second factor from

$$v(\lambda, \mathbf{q}_i) v^*(\lambda, \mathbf{q}_f) = v(\lambda, \mathbf{q}_i - \mathbf{q}_f). \qquad (4.8)$$

Note that the $\mathbf{q}$ dependence of $\hat{M}$ does not have the periodicity with the MBZ, leading to RIXS intensities that are different between inside and outside the first MBZ.

B. Correlation function within the RPA

To evaluate the correlation function, it is convenient to introduce the time-ordered Green's function,

$$[\hat{Y}^{\mathrm{T}}(q)]_{\xi_1\xi_1'; \xi\xi'} = -i \int \langle T\{[\rho_{\mathbf{q}\xi_1\xi_1'}(t)]^\dagger \rho_{\mathbf{q}\xi\xi'}(0)\} \rangle e^{iq_0 t} dt. \quad (4.9)$$

The correlation function is evaluated from the Green's function by applying the fluctuation-dissipation theorem for $\omega > 0$ [38],

$$[\hat{Y}^{+-}(q)]_{\xi_1\xi_1'; \xi\xi'} = -i\{[\hat{Y}^{\mathrm{T}}(q)]^*_{\xi\xi'; \xi_1\xi_1'} - [\hat{Y}^{\mathrm{T}}(q)]_{\xi_1\xi_1'; \xi\xi'}\}. \quad (4.10)$$

Taking account of the multiple scattering between the particle-hole pair within the RPA, the Green's function is expressed as

$$\hat{Y}^{\mathrm{T}}(q) = \hat{F}(q)[\hat{I} + \hat{\Gamma}\hat{F}(q)]^{-1} = [\hat{F}(q)^{-1} + \hat{\Gamma}]^{-1}, \quad (4.11)$$

where

$$[\hat{\Gamma}]_{\xi_2\xi_2'; \xi_1\xi_1'} = \Gamma^{(0)}(\xi_2\xi_1'; \xi_1\xi_2'), \qquad (4.12)$$

and the particle-hole propagator $\hat{F}(q)$ is defined as

$$[\hat{F}(q)]_{\xi_2\xi_2'; \xi_1\xi_1'} \equiv -i\frac{2}{N} \sum_{\mathbf{k}} \int \frac{dk_0}{2\pi} [\hat{G}(\mathbf{k} + \mathbf{q}, k_0 + \omega)]_{\xi_2\xi_1}$$

$$\times [\hat{G}(\mathbf{k}, k_0)]_{\xi_1'\xi_2'}. \qquad (4.13)$$

By substituting Eq. (2.14) into the single-particle Green's function, we get

$$[\hat{F}(q)]_{\xi_2\xi_2'; \xi_1\xi_1'}$$

$$= \frac{2}{N} \sum_{\mathbf{k}} \sum_{\ell, \ell'} U_{\xi_2\ell}(\mathbf{k} + \mathbf{q}) U_{\xi_1\ell}^*(\mathbf{k} + \mathbf{q}) U_{\xi_1'\ell'}(\mathbf{k}) U_{\xi_2'\ell'}^*(\mathbf{k})$$

$$\times \left[\frac{[1 - n_\ell(\mathbf{k} + \mathbf{q})] n_{\ell'}(\mathbf{k})}{\omega - E_\ell(\mathbf{k} + \mathbf{q}) + E_{\ell'}(\mathbf{k}) + i\delta} \right.$$

$$\left. - \frac{n_\ell(\mathbf{k} + \mathbf{q})[1 - n_{\ell'}(\mathbf{k})]}{\omega - E_\ell(\mathbf{k} + \mathbf{q}) + E_{\ell'}(\mathbf{k}) - i\delta} \right]. \qquad (4.14)$$

We need a special care for the bound states, which appear below the energy continuum as a pole in $\hat{Y}^{\mathrm{T}}(q)$. For the bound state $\omega > 0$, since $\hat{F}(q)$ is a Hermitian matrix, we could diagonalize $\hat{F}(q)^{-1} + \hat{\Gamma}$ by a unitary matrix. Let an eigenvalue be zero at $\omega = \omega_B(\mathbf{q})$ with the eigenvector $B_{\xi\xi'}(\mathbf{q})$. We could expand $[\hat{Y}^{\mathrm{T}}(q)]_{\xi_1\xi_1'; \xi\xi'}$ around $\omega = \omega_B(\mathbf{q})$ as

$$[\hat{Y}^{\mathrm{T}}(q)]_{\xi_1\xi_1'; \xi\xi'} = \frac{[\hat{C}(\mathbf{q})]_{\xi_1\xi_1'; \xi\xi'}}{\omega - \omega_B(\mathbf{q}) + i\delta}, \qquad (4.15)$$
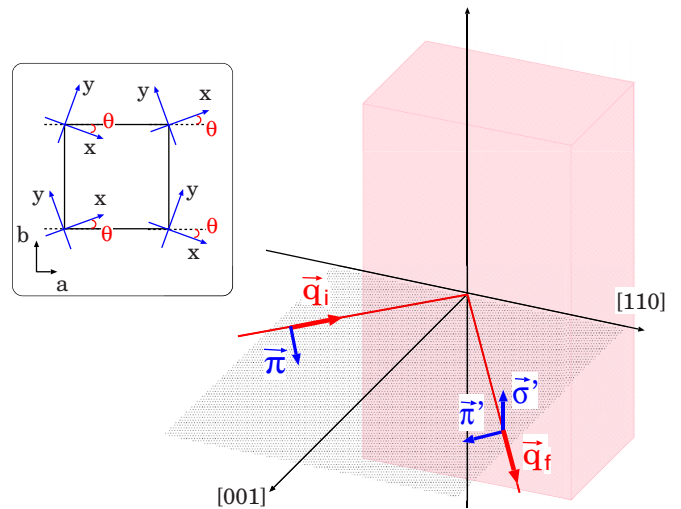

FIG. 2. (Color online) Geometry of 90° scattering. The scattering plane is perpendicular to the *ab* plane and intersects the plane along the [110] direction. The inset depicts the local coordinate frames, which are rotated by angle $\pm\theta$ around the *c* axis.
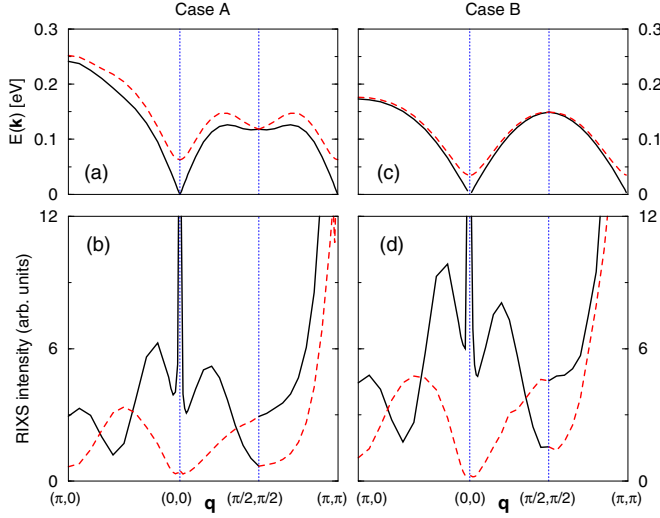
FIG. 3. (Color online) Dispersion relation of a magnon and the corresponding RIXS intensity for **q** along symmetry directions. (a) and (b) are for the parameters in case A, while (c) and (d) are in case B. The (black) solid and (red) dotted lines are for the modes with lower and higher energies, respectively.

where

$$[\hat{C}(\mathbf{q})]_{\xi_1\xi_1';\xi\xi'} = \frac{B_{\xi_1\xi_1'}(\mathbf{q})B_{\xi\xi'}^*(\mathbf{q})}{\sum_{\xi_2\xi_2'\xi_3\xi_3'} B_{\xi_3\xi_3'}^*(\mathbf{q}) \frac{\partial[\hat{F}(\mathbf{q},\omega_B(\mathbf{q}))^{-1}]_{\xi_3\xi_3';\xi_2\xi_2'}}{\partial\omega} B_{\xi_2\xi_2'}(\mathbf{q})}. \tag{4.16}$$

The correlation function is evaluated by inserting (4.15) into the right hand side of Eq. (4.10), which results in

$$\hat{Y}^{+-}(q) = 2\pi\hat{C}(\mathbf{q})\delta(\omega - \omega_B(\mathbf{q})). \tag{4.17}$$

Finally, the contribution to the RIXS intensity from the bound state is given by substituting Eq. (4.17) into Eq. (4.4).

V. NUMERICAL RESULTS FOR RIXS SPECTRA

We consider the specific case of a 90° scattering angle in accordance with the experiments. The scattering plane is perpendicular to the IrO_2 plane, which intersects the ab plane with the [110] direction, as illustrated in Fig. 2. Since $\omega \sim 11.2$ keV and $|\mathbf{q}_i| \sim 5.7$ Å^{-1} at the Ir L_3 edge, only a few degrees of tilt of the scattering plane could sweep the entire Brillouin zone. The local coordinate frame is defined by rotating the xy axes around the crystal c axis with $\theta = 11°$ ($-11°$) at the A (B) sublattice, as shown in the inset of Fig. 2. Therefore the polarization vectors are represented in the local coordinate frames as

$$\alpha_i : \pi = \left(\frac{\cos\theta \mp \sin\theta}{2}, \frac{\cos\theta \pm \sin\theta}{2}, \frac{1}{\sqrt{2}}\right), \tag{5.1}$$

$$\alpha_f : \sigma' = \left(\frac{\cos\theta \pm \sin\theta}{\sqrt{2}}, \frac{-\cos\theta \pm \sin\theta}{\sqrt{2}}, 0\right), \tag{5.2}$$

$$: \pi' = \left(-\frac{\cos\theta \mp \sin\theta}{2}, -\frac{\cos\theta \pm \sin\theta}{2}, \frac{1}{\sqrt{2}}\right), \tag{5.3}$$
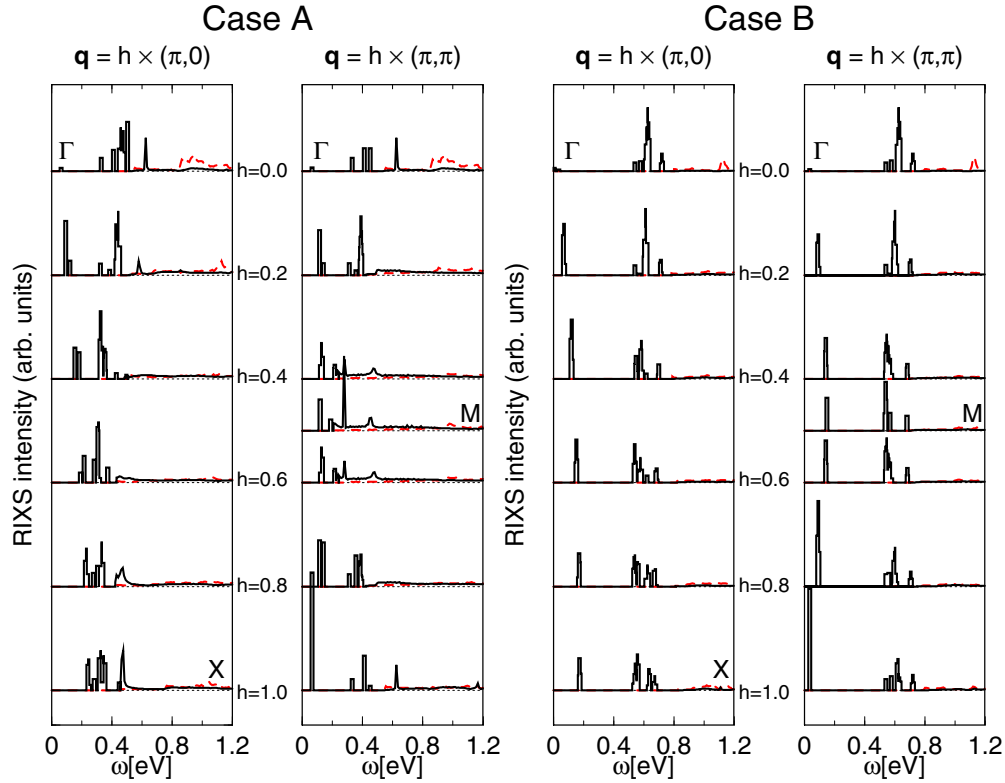

FIG. 4. (Color online) The RIXS spectra as a function of energy loss ω for **q** along symmetry directions. The (black) solid and (red) dashed lines correspond to the intensities with and without taking account of the multiple scattering, respectively. The δ-function peaks are replaced by rectangles with their widths 0.02 eV.

where the upper and lower signs correspond to the A and B sublattices, respectively. The incident x ray is assumed to have the π polarization. Inserting these relations into Eq. (4.7), we obtain $\hat{M}$.

A. Spectra for magnon

We first study the magnetic excitations emerging as bound states in $Y^T(q)$, which may be called magnons. We numerically evaluate $\hat{F}(q)$ by summing over **k** in Eq. (4.14) with dividing the first MBZ into 100×100 meshes. The calculation is straightforward for ω below the energy continuum. The bound states are determined by adjusting ω to give a zero eigenvalue in $\hat{F}(q)^{-1} + \hat{\Gamma}$. In evaluating the corresponding intensity, we numerically carry out a finite difference between $\omega = \omega_B(\mathbf{q})$ and $\omega_B(\mathbf{q}) + 0.01$ eV in Eq. (4.16) in place of the differentiation.

Figure 3 shows the dispersion relation of a magnon thus determined, and the corresponding RIXS intensities at the L_3 edge. It is found that the magnon is split into two modes with slightly different energies, as already reported [32]. Although such split modes are not confirmed, their dispersion relation is in qualitative agreement with that derived from the RIXS experiment. In case A, the energies of the magnon are given by $\omega_B(\pi,0) = 0.241$ and 0.252 eV at the X point, while $\omega_B(\pi/2,\pi/2) = 0.118$ eV at the M point, which slightly overestimates the magnon energies. On the other hand, in case B, we have $\omega_B(\pi,0) = 0.173$ and 0.176 eV at the X point, and $\omega_B(\pi/2,\pi/2) = 0.149$ eV at the M point, which slightly underestimates the magnon energies.

The RIXS intensity at the L_3 edge is also shown in Fig. 3. Although the energy of the magnon is periodic with the MBZ, the intensity is not periodic because of the presence of $v(\mathbf{q})$ in Eq. (4.7). In the narrow region around the Γ point, the intensity of the mode with lower energy seems to diverge with $|\mathbf{q}| \to 0$. This arises from the staggered rotation of the IrO_6 octahedra, and may be related to the presence of weak ferromagnetism. The intensity of another mode [$\omega_B(0) = 0.057$ eV in case A and 0.035 eV in case B] is weak but finite. On the other hand, around the $\mathbf{q} = (\pi,\pi)$, the intensity of the mode with lower energy diverges with $\mathbf{q} \to (\pi,\pi)$, due to a reflection of the antiferromagnetic order. The intensity of another mode with higher energy is finite but quite large. Although the magnon peak at the X point has been interpreted as being separated into a one-magnon peak and a weak two-magnon peak in the RIXS experiment [see Fig. 4(c) in Ref. [17]], it might be more appropriate to assign the two peaks as the split modes, since the intensities of the two-magnon excitations are expected to be quite small. At the M point, the separation of the intensity could not be perceived, since the two modes are degenerate. It is found from the intensity curve that, across the M point, the wave function of the mode with low energy is continuously connected to that with higher energy and vice versa. These characteristics mentioned above are consistent with the recent analysis on the basis of the localized spin model [23]. For the general values of **q**, however, the intensity varies rather strongly with changing values of **q**, in contrast with the monotonic change found in the localized spin model.
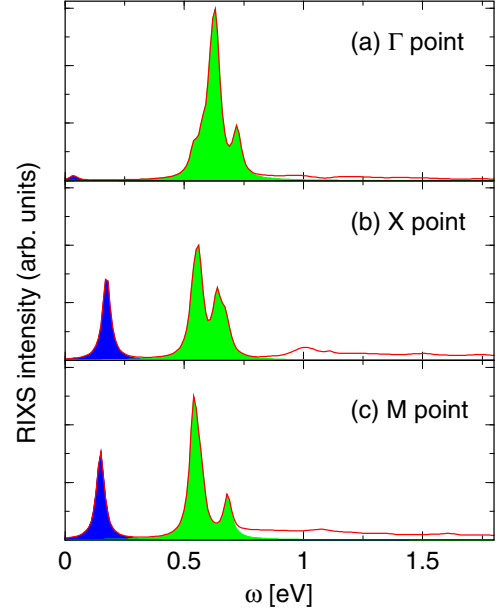

FIG. 5. (Color online) The RIXS spectra for both the magnon and exciton excitations as a function of energy loss ω at (a) the Γ, (b) X, and (c) M points, with $\zeta_{SO} = 0.45$ eV and $t_1 = 0.25$ eV (case B). The spectra are convoluted with a Lorentzian function with a full width at half maximum of 0.04 eV. The (blue) solid area around the peak with the lowest energy represents the magnon contribution. The contribution from the bound state of the exciton is represented by the (green) solid area around $\omega \simeq 0.5$–0.7 eV. The divergent intensities at $\omega = 0$ are excluded at the Γ point.

B. Spectra for exciton

There emerge several bound states between the magnon modes and the continuous states in the spectral function of the two-particle Green's function. The calculation of the bound states is the same as that of the magnon modes. For ω inside the energy continuum of electron-hole pair excitations, we evaluate Eq. (4.14) by storing each $E_\ell(\mathbf{k} + \mathbf{q}) - E_{\ell'}(\mathbf{k})$ into segments with a width of 0.01 eV for 100×100 **k** points, resulting in the histogram representation of the imaginary part of $\hat{F}(q)$. Setting ω at the center of each segment, we evaluate Eq. (4.14) and thereby Eq. (4.11), and finally Eq. (4.1).

Figure 4 shows the RIXS spectra thus evaluated as a function of ω for **q** along typical symmetry directions. The spectra are also shown without taking account of the multiple scattering [$\hat{Y}^T(q)$ is replaced by $\hat{F}(q)$] for reference. The δ-function peaks are replaced by rectangles with their widths 0.02 eV. It is found that the bound states bear a large part of the exciton intensities. The exciton peaks are close to the magnon peaks around the X and M points in case A, while they are well separated from the magnon peaks in case B, in agreement with the RIXS experiment. Since the bound states of the excitons are composed mainly of the $j_{eff} = 1/2$ states of an electron and $j_{eff} = 3/2$ states of a hole, the larger value of ζ_{SO} in case B may lead to a larger separation between the exciton and magnon peaks. In the localized electron picture, the exciton peak is given by the excitation from the $j_{eff} = 3/2$ manifold to the $j_{eff} = 1/2$ manifold, where the dispersion is given by the hopping in the antiferromagnetic isospin background [22,29].

For comparison with the experimental RIXS spectra, the calculated spectra are convoluted with the Lorentzian function with a full width half maximum 0.04 eV. Figure 5 shows the result in case B. The peak with the lowest energy represents the magnon contribution. The intensity diverging at $\omega = 0$ is excluded at the Γ point. The split of the magnon modes could not be distinguished at the X point due to the convolution. The intensities of the exciton peaks are two or three times larger than those of the magnon modes, whose ratio is comparable with the experiment [17].

VI. CONCLUDING REMARKS

We have analyzed the L-edge RIXS spectra from Sr_2IrO_4 in an itinerant-electron approach. Introducing a multiorbital tight-binding model, we have calculated the one-electron energy band within the HFA, and the Green's functions for particle-hole pair excitations within the RPA. The RIXS spectra have been evaluated from the Green's functions within the FCA. We have found two kinds of peaks in the RIXS spectra.

One is the peak of the magnon, which arises from the bound state in $\hat{Y}^{\mathrm{T}}(q)$. The dispersion of the magnon is obtained in agreement with the experiment [17]. We have predicted two-peak structures with a slightly different excitation energy

$\sim$0.05 eV due to the split of the magnon modes. Since the instrumental resolution is the same order as the split, it seems hard to detect the split in RIXS experiments. Some clue of the split, however, might be found with a careful examination of the spectral shape or by improving the experimental energy resolution.

Another is the peak of the exciton, which also arises from the bound states in $\hat{Y}^{\mathrm{T}}(q)$. We have found large intensities concentrated on these peaks in comparison with the intensities of the continuous states. The peak positions relative to the magnon peaks depend on parameters. The larger value of ζ_{SO} and the smaller value of t_1 (case B) seem to give exciton peaks that are in a better position in comparison to the RIXS experiment. To make a quantitative understanding of the spectra, however, it may be necessary to refine the present model by including the hopping electron to further neighbors as well as the tetragonal crystal field or by including more correlation effects beyond the HFA and RPA. Studies along this direction are left for the future.

[1] L. J. P. Ament, M. van Veenendaal, T. P. Devereaux, J. P. Hill, and J. van den Brink, Rev. Mod. Phys. **83**, 705 (2011).

[2] K. Ishii, T. Tohyama, and J. Mizuki, J. Phys. Soc. Jpn. **82**, 021015 (2013).

[3] T. Nagao and J. I. Igarashi, Phys. Rev. B **75**, 214414 (2007).

[4] J. van den Brink, Europhys. Lett. **80**, 47003 (2007).

[5] J. P. Hill, G. Blumberg, Y. -J. Kim, D. S. Ellis, S. Wakimoto, R. J. Birgeneau, S. Komiya, Y. Ando, B. Liang, R. L. Greene *et al.*, Phys. Rev. Lett. **100**, 097001 (2008).

[6] F. Forte, L. J. P. Ament, and J. van den Brink, Phys. Rev. B **77**, 134428 (2008).

[7] L. Braicovich, L. J. P. Ament, V. Bisogni, F. Forte, C. Aruta, G. Balestrino, N. B. Brookes, G. M. D. Luca, P. G. Medaglia, F. M. Granozio *et al.*, Phys. Rev. Lett. **102**, 167401 (2009).

[8] L. Braicovich, J. van den Brink, V. Bisogni, M. M. Sala, L. J. P. Ament, N. B. Brookes, G. M. De Luca, M. Salluzzo, T. Schmitt, V. N. Strocov *et al.*, Phys. Rev. Lett. **104**, 077002 (2010).

[9] M. Guarise, B. D. Piazza, M. M. Sala, G. Ghiringhelli, L. Braicovich, H. Berger, J. N. Hancock, D. van der Marel, T. Schmitt, V. N. Strocov *et al.*, Phys. Rev. Lett. **105**, 157006 (2010).

[10] L. J. P. Ament, F. Forte, and J. van den Brink, Phys. Rev. B **75**, 115118 (2007).

[11] L. J. P. Ament, G. Ghiringhelli, M. M. Sala, L. Braicovich, and J. van den Brink, Phys. Rev. Lett. **103**, 117003 (2009).

[12] M. W. Haverkort, Phys. Rev. Lett. **105**, 167404 (2010).

[13] J. I. Igarashi and T. Nagao, Phys. Rev. B **85**, 064421 (2012).

[14] J. I. Igarashi and T. Nagao, Phys. Rev. B **85**, 064422 (2012).

[15] T. Nagao and J. I. Igarashi, Phys. Rev. B **85**, 224436 (2012).

[16] K. Ishii, I. Jarrige, M. Yoshida, K. Ikeuchi, J. Mizuki, K. Ohashi, T. Takayama, J. Matsuno, and H. Takagi, Phys. Rev. B **83**, 115121 (2011).

[17] J. Kim, D. Casa, M. H. Upton, T. Gog, Y.-J. Kim, J. F. Mitchell, M. van Veenendaal, M. Daghofer, J. van den Brink, G. Khaliullin *et al.*, Phys. Rev. Lett. **108**, 177003 (2012).

[18] M. K. Crawford, M. A. Subramanian, R. L. Harlow, J. A. Fernandez-Baca, Z. R. Wang, and D. C. Johnston, Phys. Rev. B **49**, 9198 (1994).

[19] G. Cao, J. Bolivar, S. McCall, J. E. Crow, and R. P. Guertin, Phys. Rev. B **57**, R11039 (1998).

[20] S. J. Moon, M. W. Kim, K. W. Kim, Y. S. Lee, J.-Y. Kim, J.-H. Park, B. J. Kim, S.-J. Oh, S. Nakatsuji, Y. Maeno *et al.*, Phys. Rev. B **74**, 113104 (2006).

[21] G. Jackeli and G. Khaliullin, Phys. Rev. Lett. **102**, 017205 (2009).

[22] L. J. P. Ament, G. Khaliullin, and J. van den Brink, Phys. Rev. B **84**, 020403 (2011).

[23] J. I. Igarashi and T. Nagao, Phys. Rev. B **89**, 064410 (2014).

[24] M. O. Krause and J. H. Oliver, J. Phys. Chem. Ref. Data **8**, 329 (1979).

[25] V. M. Katukuri, H. Stoll, J. van den Brink, and L. Hozoi, Phys. Rev. B **85**, 220402(R) (2012).

[26] J. I. Igarashi and T. Nagao, Phys. Rev. B **88**, 104406 (2013).

[27] R. Arita, J. Kuneš, A. V. Kozhevnikov, A. G. Eguiluz, and M. Imada, Phys. Rev. Lett. **108**, 086403 (2012).

[28] S. Moser, L. Moreschini, A. Ebrahimi, B. D. Piazza, M. Isobe, H. Okabe, J. Akimitsu, V. V. Mazurenko, K. S. Kim, A. Bostiwick *et al.*, New J. Phys. **16**, 013008 (2014).

[29] B. H. Kim, G. Khaliullin, and B. I. Min, Phys. Rev. Lett. **109**, 167205 (2012).

[30] B. J. Kim, H. Jin, S. J. Moon, J.-Y. Kim, B.-G. Park, C. S. Leem, J. Yu, T. W. Noh, C. Kim, S.-J. Oh *et al.*, Phys. Rev. Lett. **101**, 076402 (2008).

[31] H. Watanabe, T. Shirakawa, and S. Yunoki, Phys. Rev. Lett. **105**, 216410 (2010).

[32] J. I. Igarashi and T. Nagao, J. Phys. Soc. Jpn. **83**, 053709 (2014).

[33] There exist several bound states between the magnon modes and the continuous states, which have been missed in Ref. [32].

[34] F. Wang and T. Senthil, Phys. Rev. Lett. **106**, 136402 (2011).

[35] J. Kanamori, Prog. Theor. Phys. **30**, 275 (1963).

[36] H. Watanabe, T. Shirakawa, and S. Yunoki, Phys. Rev. Lett. **110**, 027002 (2013).

[37] N. B. Perkins, Y. Sizyuk, and P. Wölfle, Phys. Rev. B **89**, 035143 (2014).

[38] J. I. Igarashi and T. Nagao, Phys. Rev. B **88**, 014407 (2013).

[39] B. J. Kim, H. Ohsumi, T. Komesu, S. Sakai, T. Morita, H. Takagi, and T. Arima, Science **323**, 1329 (2009).

[40] J. P. Clancy, N. Chen, C. Y. Kim, W. F. Chen, K. W. Plumb, B. C. Jeon, T. W. Noh, and Y. -J. Kim, Phys. Rev. B **86**, 195131 (2012).